IEICE Electronics Express, Vol.16, No.10, 1–6

LETTER

Analytic analysis for effects of input initial phase on input-output dynamics of memristor

Wei Hu[1], **Rongshan Wei**[1], **and Jinbiao Lin**[1,2a)]

Abstract The analytic expressions of input-output dynamic parameters of memristor (i.e., state variable, memristance, and output response) with respect to initial phase of sinusoidal input are obtained by using Homotopy Analysis Method (HAM). Furthermore, a new exponent, called Response Time Delay (difference) between the Maximum Values of input and output—RDMV-IO, is proposed to rapidly analyze the memristor input-output dynamics, under different initial phases. Employing RDMV-IO, we further reveal the intrinsic relationship between initial phase and dynamics. The studies are verified by using Mathematica simulations adopting nonlinear dopant drift memristor model coupled with window function.

Keywords: memristor, input-output dynamics, initial phase, analytic, HAM

Classification: Integrated circuits

1. Introduction

Since the successful development of the Hewlett-Packard (HP) prototype device [1], memristor has drawn a great deal of research interests [2]. It has been widely used in embedded memory [3, 4], neurobiology [5, 6], artificial intelligence [7], neural networks [8, 9], etc., due to the following advantages: fast speed [10], high density [11], and low power consumption [12, 13]. Memristor is a category of nano-devices with nonlinear input-output dynamics. The memristor input-output dynamics are the transient evolutions of dynamic parameters, such as state variable, memristor resistance (referred to as memristance), and output response. The dynamics depend greatly on the state variable that is controlled by the history of input excitation [1], due to the fact that the state variable is a core parameter of memristor which controls the other dynamic parameters. Therefore, the input-output dynamics is significantly affected by the amplitude, frequency, and initial phase of input excitation [14].

Many studies [1, 15, 16, 17, 18, 19] have focused on the effects of the amplitude and frequency of sinusoidal input on memristor input-output dynamics. However, by definition, the initial phases of the inputs were ignored or assumed to be 0° in order to simplify these studies.

Even worse, the commonly used numerical simulations in these studies may cause serious truncation and rounding errors [20]. By contrast, analytic analysis is capable of overcoming these errors and enabling ones to implement deep theoretical investigations and performance predictions of memristor [19]. Moreover, the analytic expressions can be conveniently integrated into EDA tools, which facilitate the commercial applications of memristor [18].

Unfortunately, there are few analytic studies in the effect of input initial phase on the memristor input-output dynamics so far. Elashkar has investigated the influences of the initial phase of sinusoidal input on the transient memristance and I-V Pinched Hysteresis Loop (PHL) of memristor, and has derived the analytic expression of transient memristance [21]. However, besides the transient memristance, the analytic expressions of other dynamic parameters (i.e., state variable, average state variable, average memristance, and output response), as functions of the initial phase, are also considerably important for theoretical analyses of evaluations of the memristor input-output dynamics. In fact, these expressions were not given in [21]. Additionally, Elashkar has adopted a memristor model without coupling a nonlinear window function for memristance analyses [21], resulting in the analyses did not fully exhibit actual physical characteristics. Liu has explored the curves of transient memristance with various initial phases in [22], where the used memristor models are based on the simple piece-wise linear and cubic mathematical models rather than the actual physical model. Besides, the analytic expressions of dynamic parameters were not derived in [23], limiting the practical applications of the results.

To address the above limitations, *Homotopy Analysis Method* (HAM) [23, 24] is employed in this paper to analytically study the effects of the initial phase of sinusoidal input on memristor input-output dynamics. Without sacrificing the generality, the widely used HP physical model [1] coupling with the nonlinear window function [25] is adopted for representing actual physical characteristics. To be specific, firstly, HAM is used to solve the state equation of HP physical model under different input initial phases for obtaining approximate analytic solution of state variable. This is because the state variable is a core parameter of HP memristor that controls the other dynamic parameters, and hence the input-output dynamics. Then, the solved state variable is employed to derive the approximate analytic expressions of average state variable, transient memristance, average memristance, and I-V PHL. Finally, based on the traditional I-V PHL area and the

[1]School of Physics and Information Engineering, Fuzhou University, Fuzhou, Fujian 350116, China
[2]Marine Engineering College, Jimei University, Xiamen, Fujian 361021, China
a) linjinbiaojm@163.com

DOI: 10.1587/elex.16.20190154
Received March 13, 2019
Accepted March 28, 2019
Publicized April 16, 2019
Copyedited May 25, 2019

newly proposed Response Time Delay (difference) between Maximum Values of input and output (RDMV-IO), we further reveal the intrinsic relationship between the input initial phase and the memristor input-output dynamics. All the solved parameters above have the advantages of closed-form expression and symbolic computation due to the HAM. To the best of the authors' knowledge, this is the first paper that HAM is applied to analyze the effects of the initial phase of sinusoidal input on the memristor input-output dynamics.

2. Study effects of initial phase on state variable x by HAM

We first study effects of initial phase on state variable x by HAM because x is the core parameter of memristor that controls the other dynamic parameters (such as voltage V_M, memristance R_M). Based upon the original physical model of HP memristor [1], the port equation, memristance, and state equation of memristor with respect to input initial phase can be expressed by

$$V_M(t,\theta_0) = R_{\mathrm{M}}(t,\theta_0) \times I_{\mathrm{M}}(t,\theta_0) \tag{1}$$

$$\begin{aligned} R_M(t,\theta_0) &= R_{ON}x(t,\theta_0) + R_{OFF}[1 - x(t,\theta_0)] \\ &= x_N(t,\theta_0)(1-\alpha)R_{ON} + \alpha R_{ON} \end{aligned} \tag{2}$$

$$\frac{dx(t,\theta_0)}{dt} = \frac{\mu_V R_{ON}}{D^2} I_M(t,\theta_0) f[x(t)] \tag{3}$$

where the state variable $x_N(t,\theta_0) = w(t,\theta_0)/D \in [0,1]$ and input current $I_M(t,\theta_0) = A\sin(\omega t + \theta_0)$, θ_0 is the initial phase. For representing the actual physical characteristics, 1) the Joglekar window function (J-window) $f[x(t)] = 1 - (2x-1)^{2P}$ [25], where P here is a positive integer, was introduced in (1), ensuring $x \in [0,1]$ and overcoming the boundary effect; 2) $P = 2$ was chosen in this work for the effect of nonlinear ion drift in the doped layer [1]. For clarity, all the definitions and values of physical parameters of HP memristor and the input used in simulations are summarized in Table I.

In our previous work, a HAM-based analytic modeling methodology for memristor was proposed [26], in which HAM was exploited for solving the state equation of memristor to obtain the N-order analytic approximate solution $x_N(t,\theta_0,\hbar)$ of state variable $x(t)$, where $N \in \mathbb{Z}$ is the *approximation order* (taking into account the approximate accuracy and simulation efficiency, we chose $N = 3$ in this work), $\hbar \in \mathbb{R}$ is the *convergence-control parameter* that used to accelerate the convergence for solving $x_N(t,\theta_0,\hbar)$. The method for solving $\hbar$ will be explained later in this section. Note the initial phase θ_0 of input is assumed to be 0° to simplify the analyses in [26] and original paper of HP memristor [1], whereas in this work it is an unknown whose effects on the memristor input-output dynamics will be systematically studied.

Based on our modeling methodology, $x_3(t,\theta_0,\hbar)$ with J-window (we chose $N = 3$ and $P = 2$, as explained above) has the following analytic expression:

$$\begin{aligned} x_3(t,\theta_0,\hbar) &= x_0 + \sum_{m=1}^{3} x_m(t,\theta_0,\hbar) \\ &= 1 + 1024\gamma 1 - 1024\gamma 1\cos(\omega t) \\ &\quad + (\gamma 3\hbar^2 + 3\hbar\gamma 3 + 43008\gamma 2 + 3\gamma 3)\cos(\theta_0) + 512\gamma 1\cos(2\theta_0) + 14336\gamma 2\cos(3\theta_0)/3 \\ &\quad - (\gamma 3\hbar^2 + 3\hbar\gamma 3 + 43008\gamma 2 + 3\gamma 3)\cos(\omega t + \theta_0) - 1024\gamma 1\cos(\omega t + 2\theta_0) - 28672\gamma 2\cos(\omega t + 3\theta_0) \\ &\quad + 14336\gamma 2\cos(2\omega t + \theta_0) + 512\gamma 1\cos(2\omega t + 2\theta_0) + 14336\gamma 2\cos(2\omega t + 3\theta_0) \\ &\quad - 14336\gamma 2\cos(3\omega t + 3\theta_0)/3 \end{aligned} \tag{4}$$

where

$$\begin{aligned} \gamma 1 &= x_0(x_0-1)(\hbar + 3/2)({x_0}^2 - x_0 + 1/2) \\ &\quad \times (x_0 - 1/2)^3\xi^2\hbar^2 \end{aligned} \tag{5}$$

$$\begin{aligned} \gamma 2 &= x_0(x_0-1)(x_0{}^2 - x_0 + 1/2)(x_0 - 1/2)^2 \\ &\quad \times ({x_0}^4 - 2{x_0}^3 + 3{x_0}^2/2 - x_0/2 + 1/28)\xi^3\hbar^3 \end{aligned} \tag{6}$$

$$\gamma 3 = 16x0(x0-1)(x0^2 - x0 + 1/2)\xi\hbar \tag{7}$$

$$\xi = \frac{\mu_{\mathrm{V}} R_{\mathrm{ON}} A}{D^2\omega} \tag{8}$$

$\gamma 1$, $\gamma 2$, $\gamma 3$, and ξ are variables used for simplification of Eq. (4).

The average N-order analytic approximate solution of $x_N(t,\theta_0,\hbar)$ over a cycle is given by

$$\overline{x_N(t,\theta_0,\hbar)} = \frac{\int_0^{2\pi/\omega} x_N(t,\theta_0,\hbar)\,dt}{2\pi/\omega} \tag{9}$$

In Eq. (4), the *convergence-control parameter* $\hbar$ is identified as a variable needed to be solved. To derive the complete analytic expression of Eq. (4), the optimal $\hbar$ corresponding to different θ_0, which used to accelerate the convergence of approximation, is solved by minimizing the *discrete squared residual error* $Em(\theta_0,\hbar)$ [23, 26]. The solved $\hbar$ are listed in Table II.

As seen from Eq. (4), the initial phase has significant effects on the mostly cosinoidal terms of state variable expression, i.e., θ_0 controls the evolution of state variable. To verify the validity of the above theoretical analysis, we performed the analytic simulations based on Eqs. (4)–(9) and compared it with numerical simulations. Note in this work all the analytic simulations were implemented by

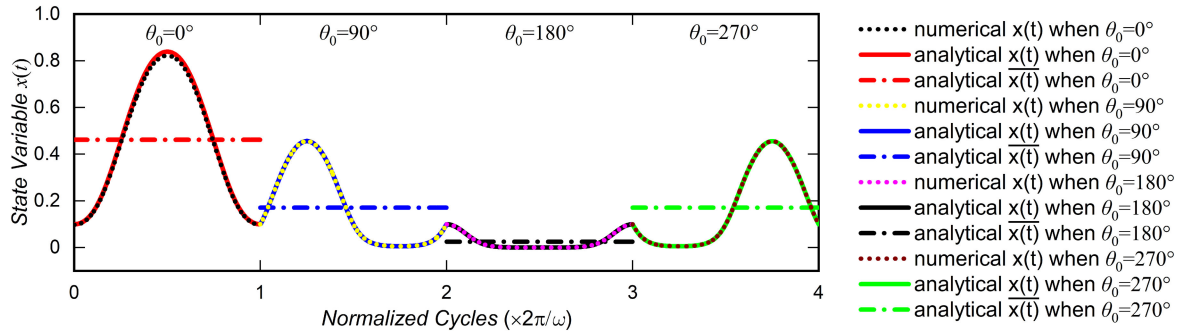

Fig. 1. Comparisons of memristor state variable x and corresponding average state variable $\bar{x}$ in 4 normalized cycles, under various initial phases. These evolutions are simulated by using the obtained analytic expressions Eqs. (4)–(9) and numerical analyses, respectively. $2\pi/\omega$ is one cycle of the sinusoidal input signal. Each θ_0 and correspondingly solved $\hbar$ are given in Table II. All the physical parameters of the HP memristor and the input parameters used in these simulations are summarized in Table I.

Table I. Physical parameters of the HP memristor and the input parameters used in simulations

Parameter	Value	Unit	Definition
D^*	10×10^{-9}	m	Thickness of the switching layer
$w(t, \theta_0)^*$	$[0, 10^{-8}]$	m	Length of the doped layer
α^*	1.6×10^2	--	Ratio of high resistance to low resistance
$R_{ON}{}^*$	10^2	Ω	Low resistance ($x = 1$)
$\mu_V{}^*$	10^{-14}	$m^2 s^{-1} V^{-1}$	Average ion mobility in small electric field
x_0	0.1	--	Initial state variable
R_0	1.4×10^4	Ω	Initial memristance
$x(t, \theta_0)$	$[0, 1]$	--	Normalized state variable, $x(t, \theta_0) = w(t, \theta_0)/D$
A	40×10^{-6}	A	Amplitude of the sinusoidal input signal
V_M	$[-\infty, \infty]$	V	Voltage across the memristor
I_M	$[-\infty, \infty]$	A	Current through the memristor
R_M	$[0, \infty]$	Ω	Memristance
ω	$[0, \infty]$	rad/s	Angular frequency of the sinusoidal input signal
T	$[0, \infty]$	s	Cycle of the sinusoidal input signal, $T = 2\pi/\omega$

*The parameter is obtained from [1].

Table II. Values of θ_0 and the corresponding optimal $\hbar$

θ_0 (°) [1]	$\hbar$ [2]	θ_0 (°) [1]	$\hbar$ [2]
0	−0.439475699	180	−0.420515742
45	−0.484572314	225	−0.466351321
90	−0.617281893	270	−0.617281893
135	−0.466351297	315	−0.838415877

[1]θ_0 is freely selected, depending on the initial phase range of the analyses.
[2]The optimal convergence-control parameter $\hbar$ can be solved by minimizing *discrete squared residual error* $Em(\theta_0, \hbar)$ [23, 26].

using the Mathematica [27], while the numerical simulations were performed by using the widely used fourth-order Runge–Kutta method.

Fig. 1 shows the comparisons of evolutions of transient state variables x and the accompanying average state variables $\bar{x}$ in four normalized input cycles. For the convenience of comparisons, each cycle has the same initial state variable x_0. The cycles are drawn for 0°, 90°, 180°, and 270° initial phases, respectively. Each initial phase corresponds to a normalized cycle. The simulation results in Fig. 1 show that:

1) our analytic simulations match the above theoretical analysis and the numerical simulations well, denoting the high accuracy of the solved analytic expression Eqs. (4)–(9). The associated Maximum Relative Error (MaxRE), Mean Relative Error (MRE), and Root Mean Square Error (RMSE) between the analytic and numerical simulation is 8.3%, 2.9%, and 0.013.
2) the variations in x and relevant $\bar{x}$ are the largest for $\theta_0 = 0°$ and are the smallest for $\theta_0 = 180°$, because the applied input current is firstly negative for $\theta_0 = 180°$, resulting in x decreases from $x_0 = 0.1$ and then reaches its boundary "0" that makes $x = 0$ and stay unchanged. While in case of 0°, the input is positive and moderate, ensuring x operates in a normal range and does not reach boundary "0" or "1", i.e., $x \in (0, 1)$. The variations in x and relevant $\bar{x}$ for 90° and 270° are mirror symmetrical, because the inputs of memristor have the opposite polarities but the same amplitudes.

To exploit the advantages of analytic analysis as mentioned in Introduction, in the following sections, we performed simulations all based on our obtained analytic expressions having high accuracy (such as Eqs. (4) and (9), as shown from x and $\bar{x}$ in Fig. 1), instead of the numerical simulations.

3. Effects of initial phase on x-controlled dynamic parameters

It is known from Section 2 that state variable x is the core of HP memristor that controls the other dynamic parameters. So that in this section, we studied the effects of initial phase θ_0 on other dynamic parameters by using x and the theoretical analyses in Section 2. This study is the foundation of input-output dynamics analysis in Section 4 and Section 5.

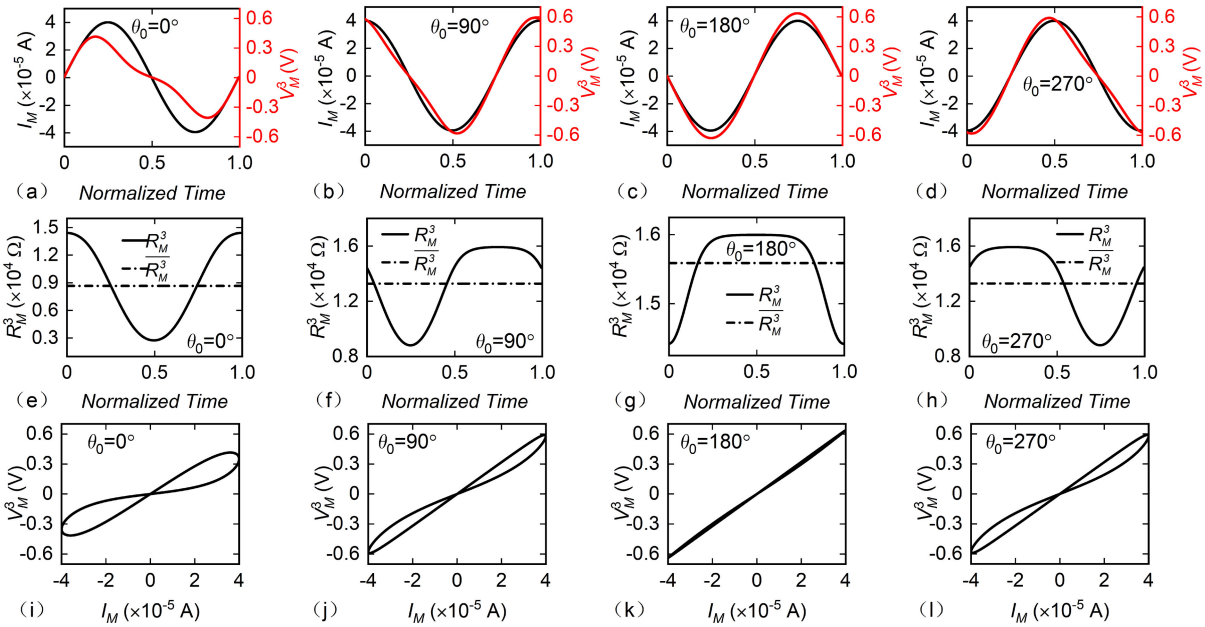

Fig. 2. Comparisons of the obtained dynamic parameters: output responses (a)–(d), memristances and average memristances (i)–(l), and I_M–V_M PHLs (i)–(l), under initial phases of 0°, 90°, 180°, and 270°, respectively. All the simulation parameters are the same as those in Fig. 1.

Based on Eqs. (1), (2), and (4), we derive the three-order analytic solution $V_M^3(t,\theta_0,\hbar)$ and $R_M^3(t,\theta_0,\hbar)$ of output response $V_M(t)$ and memristance $R_M(t)$, respectively

$$V_M^3(t,\theta_0,\hbar) = I_M(t,\theta_0) \times [x_3(t,\theta_0,\hbar)R_{ON} + \alpha(1 - x_3(t,\theta_0,\hbar))R_{ON}] \tag{10}$$

$$R_M^3(t,\theta_0,\hbar) = x_3(t,\theta_0,\hbar)R_{ON} + \alpha(1 - x_3(t,\theta_0,\hbar))R_{ON} \tag{11}$$

Then, according to Eqs. (4) and (11), the average $R_M^3(t,\theta_0,\hbar)$ over a cycle is given by

$$\overline{R_M^3(t,\theta_0,\hbar)} = \frac{\int_0^{2\pi/\omega} R_M^3(t,\theta_0,\hbar)\,dt}{2\pi/\omega} \tag{12}$$

Fig. 2 shows the evolutions of the x-controlled dynamic parameters of memristor, i.e., the output voltage V_M^3 [see Fig. 2(a), (b), (c), and (d), based on Eqs. (4) and (10)], memristance R_M^3 and average memristance $\overline{R_M^3}$ [see Fig. 2(e), (f), (g), and (h), based on Eqs. (11), (12)], and I_M–V_M PHL [see Fig. 2(i), (j), (k), and (l), based on Eqs. (4) and (10)], under four different initial phases. Note that when the initial phase is 0° and 180°, the corresponding dynamic parameters have the maximum and minimum values, respectively, similar to x and $\bar{x}$ in Fig. 1. We have found that the initial phase θ_0 has significant effects on x and $\bar{x}$ from Fig. 1. Fig. 2 further illustrates that x under different θ_0 directly controls the evolutions of the other dynamic parameters. In other words, the effects of θ_0 are transmitted to the other dynamic parameters through x. Because of this, we come to a conclusion that the initial phase θ_0 also has significant effects on the dynamic parameters.

4. Effects of initial phase on I_M–V_M PHL area

The method that analyzes dynamics with dynamic parameters presented in Section 3 is direct and effective. However, the workload of this traditional method is too heavy, a simple method that only use one parameter, referred to as I_M–V_M PHL area, was proposed to represent memristor input-output dynamics [28, 29]. So in this section, we discussed the effects of initial phase on the I_M–V_M PHL area.

According to the classical fingerprints of memristor [29], the PHL area, defined as the area enclosed by the closed I_M–V_M loop, is positively correlated with memristor input-output dynamics [28]. For instance, as PHL area tends to 0, the nonlinear input-output dynamics will disappear, i.e., the memristor will convert to a traditional linear resistor. The PHL area can be expressed by

$$S = \oint_{\Gamma} V_M^N(t)\,dI_M(t) \tag{13}$$

where Γ is the closed I_M–V_M loop as shown in Fig. 2(i), (j), (k), and (l). Substituting the given $I_M(t,\theta_0)$ into (13), the analytic expression of PHL area is

$$S(\theta_0) = 2\int_0^{\pi/\omega} V_M^N(t,\theta_0)A\omega\cos(\omega t)\,dt \tag{14}$$

Combing Eqs. (1), (2), and (11), we can obtain the analytical expression of Eq. (14). Then the quantitative analysis in Fig. 3 shows that the PHL area increases first and then decreases with the increasing initial phase, demonstrating a U-shaped curve. This is because as θ_0 increases in $[0°, 180°]$, the variation in x decreases due to the input that is positive, leading to the decrease in variation in output and, thus, that in I_M–V_M PHL area, and vice

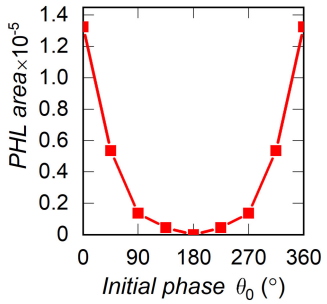

Fig. 3. Dependence of the I_M–V_M PHL area on θ_0. All the simulation parameters are the same as those in Fig. 1.

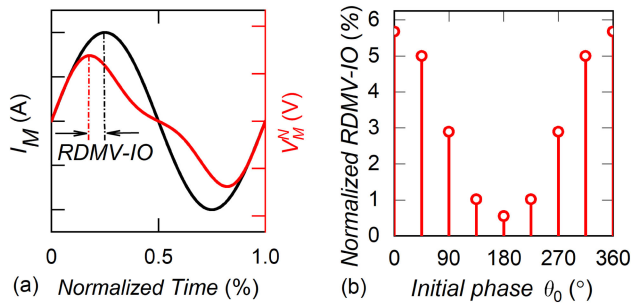

Fig. 4. (a) Definition of RDMV-IO and (b) dependence of the normalized RDMV-IO on θ_0. Normalized time = time/$T \times 100\%$. All the simulation parameters are the same as those in Fig. 1.

versa in $[180°, 360°]$. Since PHL area is positively correlated with memristor input-output dynamics, the observation in Fig. 3 indicates θ_0 and the dynamics also have a U-shaped relation. Note that when θ_0 is 0° (or 360°) and 180°, the corresponding PHL areas have the minimum and maximum values, indicating the strongest and the weakest input-output dynamics, respectively.

5. RDMV-IO

Although using the I_M–V_M PHL area to analyze the memristor input-output dynamics is indeed a simpler method compared with using dynamic parameters, this method is quite inconvenient and easy to cause error for practical measurement (which we shall explain bellow). Thus, we propose a novel method here for analyzing the input-output dynamics by the Response Time Delay (difference) between Maximum Values of input and output in one cycle (RDMV-IO), a graphical interpretation of RDMV-IO is shown in Fig. 4(a).

Clearly, the measurement of RDMV-IO is more convenient than that of PHL area. This is because we only need to measure the times corresponding to the maximum values of the input and output, and then simply subtract these two times to achieve RDMV-IO extraction. Nevertheless, measuring the PHL area requires not only real-time measurement of a large number of transient values of the input and output, but also the storage of these values. Finally, mathematical software is needed to numerically calculate the specific I_M–V_M PHL area. Therefore, analyzing input-output dynamics by RDMV-IO is an easy-to-measure method.

To verify the validity of RDMV-IO, we performed the simulation as shown in Fig. 4(b). It is clear from Fig. 4(b) that as the initial phase increases, the normalized RDMV-IO ($|\text{RDMV-IO}/T| \times 100\%$) increases firstly and then decreases, similar to the PHL area-initial phase curve in Fig. 3. This observation suggests that RDMV-IO, like PHL area, is also positively correlated with the input-output dynamics of memristor. Therefore, with the conveniences of RDMV-IO mentioned before, we can rapidly and easily analyze the effects of initial phase on the input-output dynamics of memristor. The physical mechanism of RDMV-IO may be contributed to the moving time of doped layer, microscopically, due to drift or diffusion time of ion [30].

6. Discussion

After fabricating memristor, its input-output dynamics depend only on input signals of applications. Therefore, the analysis method in this paper can be employed for evaluation and prediction of memristor performance, which is particularly useful for applications that need to enhance dynamics (the larger RDMV-IO the better) or to avoid the disappearance of dynamics (i.e., RDMV-IO = 0).

It should be noted that, although our research subject is the HP memristor with J-window under sinusoidal input current, the analytic analysis method of the memristor input-output dynamics can be easily extended to other types of novel memory devices, window functions, and inputs (e.g., triangular voltage), due to the generality of HAM [23, 24] to solve *Nonlinear Differential Algebraic Equation* regarding core parameter of device (such as the state variable in HP memristor).

7. Conclusion

In summary, we have analytically analyzed the effects of initial phase of sinusoidal input on memristor input-output dynamics by employing the HAM and the newly proposed RDMV-IO. We found that the input initial phase has significant effects on the dynamics parameters. Base on these results, we further reveal that the memristor input-output dynamics are affected by the increasing input initial phase, demonstrating a U-shaped relationship.

References

[1] D. B. Strukov, *et al.*: "The missing memristor found," Nature **453** (2008) 80 (DOI: 10.1038/nature06932).
[2] International Technology Roadmap for Semiconductors: ITRS (2015) http://www.itrs2.net/itrs-reports.html.
[3] S. Pi, *et al.*: "Memristor crossbar arrays with 6-nm half-pitch and 2-nm critical dimension," Nat. Nanotechnol. **14** (2019) 35 (DOI: 10.1038/s41565-018-0302-0).
[4] H. Abbas, *et al.*: "A memristor crossbar array of titanium oxide for non-volatile memory and neuromorphic applications," Semicond. Sci. Technol. **32** (2017) 065014 (DOI: 10.1088/1361-6641/aa6a3a).
[5] Y. van de Burgt, *et al.*: "A non-volatile organic electrochemical device as a low-voltage artificial synapse for neuromorphic computing," Nat. Mater. **16** (2017) 414 (DOI: 10.1038/nmat4856).
[6] P. M. Sheridan, *et al.*: "Sparse coding with memristor networks," Nat. Nanotechnol. **12** (2017) 784 (DOI: 10.1038/nnano.2017.83).
[7] W. H. Chen, *et al.*: "A 65 nm 1 Mb nonvolatile computing-in-

memory ReRAM macro with sub-16 ns multiply-and-accumulate for binary DNN AI edge processors," IEEE ISSCC Dig. Tech. Paper (2018) Start Page (DOI: 10.1109/ISSCC.2018.8310400).
[8] J. Cao and R. Li: "Fixed-time synchronization of delayed memristor-based recurrent neural networks," Sci. China Inf. Sci. **60** (2017) 032201 (DOI: 10.1007/s11432-016-0555-2).
[9] Y. Chen, *et al.*: "A novel memristor-based restricted Boltzmann machine for contrastive divergence," IEICE Electron. Express **15** (2018) 20171062 (DOI: 10.1587/elex.15.20171062).
[10] B. J. Choi, *et al.*: "High-speed and low-energy nitride memristors," Adv. Funct. Mater. **26** (2016) 5290 (DOI: 10.1002/adfm.201600680).
[11] Q. Luo, *et al.*: "Self-rectifying and forming-free resistive-switching device for embedded memory application," IEEE Electron Device Lett. **39** (2018) 664 (DOI: 10.1109/LED.2018.2821162).
[12] P. Bousoulas, *et al.*: "Low-power forming free $TiO_{2-x}/HfO_{2-y}/TiO_{2-x}$-trilayer ReRAM devices exhibiting synaptic property characteristics," IEEE Trans. Electron Devices **64** (2017) 3151 (DOI: 10.1109/TED.2017.2709338).
[13] J. Zhou, *et al.*: "Very low-programming-current RRAM with self-rectifying characteristics," IEEE Electron Device Lett. **37** (2016) 404 (DOI: 10.1109/LED.2016.2530942).
[14] Z. Biolek, *et al.*: "Spice model of memristor with nonlinear dopant drift," Radioengineering **18** (2009) 210.
[15] S. Ali, *et al.*: "Flexible frequency selective passive circuits based on memristor and capacitor," Org. Electron. **51** (2017) 119 (DOI: 10.1016/j.orgel.2017.09.012).
[16] A. Rodriguez-Fernandez, *et al.*: "Effect of the voltage ramp rate on the set and reset voltages of ReRAM devices," Microelectron. Eng. **178** (2017) 61 (DOI: 10.1016/j.mee.2017.04.039).
[17] S. Asapu and T. Maiti: "Multifilamentary conduction modeling in transition metal oxide-based RRAM," IEEE Trans. Electron Devices **64** (2017) 3145 (DOI: 10.1109/TED.2017.2709249).
[18] I. Messaris, *et al.*: "A data-driven Verilog-A ReRAM model," IEEE Trans. Comput.-Aided Des. Integr. Circuits Syst. **37** (2018) 3151 (DOI: 10.1109/tcad.2018.2791468).
[19] S. Thomas and S. Prakash: "An accurate analytical memristor model for spice simulators," IEICE Electron. Express **15** (2018) 20180724 (DOI: 10.1587/elex.15.20180724).
[20] D. Biolek, *et al.*: "Modeling of TiO_2 memristor: From analytic to numerical analyses," Semicond. Sci. Technol. **29** (2014) 125008 (DOI: 10.1088/0268-1242/29/12/125008).
[21] N. E. Elashkar, *et al.*: "Memristor based BPSK and QPSK demodulators with nonlinear dopant drift model," Microelectron. J. **56** (2016) 17 (DOI: 10.1016/j.mejo.2016.07.015).
[22] W. Liu, *et al.*: "Exponential flux-controlled memristor model and its floating emulator," Chin. Phys. B **24** (2015) 118401 (DOI: 10.1088/1674-1056/24/11/118401).
[23] S. J. Liao: *Homotopy Analysis Method in Nonlinear Differential Equations* (Springer & Higher Education Press, Heidelberg, 2012) 135.
[24] S. J. Liao: *Advances in the Homotopy Analysis Method* (World Scientific, Singapore, 2013) 103.
[25] Y. N. Joglekar and S. J. Wolf: "The elusive memristor: Properties of basic electrical circuits," Eur. J. Phys. **30** (2009) 661 (DOI: 10.1088/0143-0807/30/4/001).
[26] W. Hu, *et al.*: "An analytic HAM-based modeling methodology for memristor enabling fast convergence," submitted to IEEE Trans. Comput.-Aided Des. Integr. Circuits Syst. (2018) Available: https://arxiv.org/abs/1812.00317.
[27] Wolfram Research: http://www.Wolfram.Com/mathematica/.
[28] Z. Biolek, *et al.*: "Computation of the area of memristor pinched hysteresis loop," IEEE Trans. Circuits Syst. II, Exp. Briefs **59** (2012) 607 (DOI: 10.1109/TCSII.2012.2208670).
[29] S. P. Adhikari, *et al.*: "Three fingerprints of memristor," IEEE Trans. Circuits Syst. I, Reg. Papers **60** (2013) 3008 (DOI: 10.1109/TCSI.2013.2256171).
[30] J. H. Yoon, *et al.*: "An artificial nociceptor based on a diffusive memristor," Nat. Commun. **9** (2018) 417 (DOI: 10.1038/s41467-017-02572-3).